JOURNAL OF GEOPHYSICAL RESEARCH, VOL. 100, NO. A7, PAGES 11,845–11,861, JULY 1, 1995

Characteristics of ionospheric convection and field-aligned current in the dayside cusp region

G. Lu,[1] L. R. Lyons,[2] P. H. Reiff,[3] W. F. Denig,[4] O. de la Beaujardiére,[5] H. W. Kroehl,[6] P. T. Newell,[7] F. J. Rich,[4] H. Opgenoorth,[8] M. A. L. Persson,[8] J. M. Ruohoniemi,[7] E. Friis-Christensen,[9] L. Tomlinson,[10] R. Morris,[11] G. Burns,[11] A. McEwin[12]

Abstract. The assimilative mapping of ionospheric electrodynamics (AMIE) technique has been used to estimate global distributions of high-latitude ionospheric convection and field-aligned current by combining data obtained nearly simultaneously both from ground and from space. Therefore, unlike the statistical patterns, the "snapshot" distributions derived by AMIE allow us to examine in more detail the distinctions between field-aligned current systems associated with separate magnetospheric processes, especially in the dayside cusp region. By comparing the field-aligned current and ionospheric convection patterns with the corresponding spectrograms of precipitating particles, the following signatures have been identified: (1) For the three cases studied, which all had an IMF with negative y and z components, the cusp precipitation was encountered by the DMSP satellites in the postnoon sector in the northern hemisphere and in the prenoon sector in the southern hemisphere. The equatorward part of the cusp in both hemispheres is in the sunward flow region and marks the beginning of the flow rotation from sunward to antisunward. (2) The pair of field-aligned currents near local noon, i.e., the cusp/mantle currents, are coincident with the cusp or mantle particle precipitation. In distinction, the field-aligned currents on the dawnside and duskside, i.e., the normal region 1 currents, are usually associated with the plasma sheet particle precipitation. Thus the cusp/mantle currents are generated on open field lines and the region 1 currents mainly on closed field lines. (3) Topologically, the cusp/mantle currents appear as an expansion of the region 1 currents from the dawnside and duskside and they overlap near local noon. When B_y is negative, in the northern hemisphere the downward field-aligned current is located poleward of the upward current; whereas in the southern hemisphere the upward current is located poleward of the downward current. (4) Under the assumption of quasi-steady state reconnection, the location of the separatrix in the ionosphere is estimated and the reconnection velocity is calculated to be between 400 and 550 m/s. The dayside separatrix lies equatorward of the dayside convection throat in the two cases examined.

[1]High Altitude Observatory, NCAR, Boulder, Colorado.
[2]The Aerospace Corporation, Los Angeles, California.
[3]Department of Space Physics and Astronomy, Rice University, Houston, Texas.
[4]Phillips Laboratory, Hanscom Air Force Base, Massachusetts.
[5]SRI, Menlo Park, California.
[6]National Geophysical Data Center, NOAA, Boulder, Colorado.
[7]Applied Physics Laboratory, Johns Hopkins University, Laurel, Maryland.
[8]Swedish Institute of Space Physics, Sweden.
[9]Danish Meteorological Institute, Copenhagen, Denmark.
[10]Institute of Geological and Nuclear Sciences, Christchurch, New Zealand.
[11]Australia Antarctic Division, Kingston, Tasmania.
[12]Australian Geological Survey Organisation, Canberra.

Paper number 94JA02665.
0148-0227/95/94JA-02665$05.00

1. Introduction

The interaction of the solar wind with the magnetosphere is the ultimate energy source for many electrodynamical phenomena in the magnetosphere and ionosphere. The plasma and momentum transfer between the solar wind and the magnetosphere can be accomplished either through a diffusion process across the boundary or through magnetic reconnection, or both [see *Cowley et al.*, 1983, and references therein], depending on the solar wind conditions and the location on the magnetopause. The boundary layer diffusion process may be important at the dawn and dusk flanks of the magnetopause, while magnetic reconnection is the dominant process at the frontside magnetopause [*Sonnerup et al.*, 1981; *Reiff*, 1984; *Lundin*, 1988, and references

therein]. During the reconnection or merging processes, the originally closed geomagnetic field lines merge with the solar magnetic field lines and become open. The solar wind electric field is transmitted along these open field lines to the ionosphere, as are the solar wind plasmas. The cusp is a region of direct entry of intense solar wind plasma, and therefore has been treated as one key to understanding the magnetopause processes. The ionospheric manifestation of the cusp injection is the energy-latitude dispersion due to the $\mathbf{E}\times\mathbf{B}$ drift of the particles as they travel from the magnetopause to the ionosphere [*Shelley et al.*, 1976; *Reiff et al.*, 1977]. Recently, quantitative criteria have been developed to identify the various particle precipitations in the dayside polar cap region [*Newell and Meng*, 1988; *Newell et al.*, 1991a, b], based on years of Defense Meteorological Satellite Program (DMSP) plasma observations.

Ionospheric convection in the dayside cusp region is directly driven by the solar wind-magnetosphere interaction. The initial motion of the newly opened field lines depends on the balance between the magnetic tension force and the forces exerted by magnetosheath flow [*Cowley et al.*, 1983]. Therefore the direction of the ionospheric flow in the vicinity of the open-closed boundary is often complicated. Theoretical models [*Crooker*, 1979; *Cowley et al.*, 1991] suggest that, for a negative IMF B_y component, magnetic merging is favored to occur along the dawn (dusk) flank of the magnetopause in the northern (southern) hemisphere. Subsequently, the newly opened magnetic field lines are dragged by the magnetic tension force duskward (dawnward). The same dependence of the dayside convection flow on B_y is observed in the ionospheric polar cap [e.g., *Heelis*, 1984; *Heppner and Maynard*, 1987; *Greenwald et al.*, 1990].

Energy transfer from the outer magnetosphere to the ionosphere is accomplished by the magnetic field-aligned currents. The statistical pattern of the distribution of the field-aligned current in the ionosphere was first developed by *Iijima and Potemra* [1976]. The pattern consists of two circular current sheets as well as a separate pair of currents in the vicinity of the cusp. The inner sheet is called the region 1 currents and the outer sheet the region 2 currents. The pair of currents located poleward of the adjacent region 1 is traditionally called "cusp currents" and flow in the direction opposite to that of the region 1 currents. In recent studies, *Bythrow et al.* [1988] and *Erlandson et al.* [1988] found that the dayside region 1 currents coincide with the cusp precipitation, while the traditional cusp currents coincide with the mantle precipitation and therefore are referred to as "mantle currents." Therefore, unlike the conventional region 1 currents which are generated mainly on closed field lines near the low-latitude boundary layer [e.g., *Sonnerup*, 1980; *Troshichev*, 1982; *Siscoe et al.*, 1991], the dayside region 1 currents associated with cusp precipitation (i.e., the cusp currents) and the mantle currents are generated on open field lines through the direct magnetic reconnection between the solar wind and geomagnetic fields [e.g., *Yamauchi et al.*, 1993; *Mei et al.*, 1994]. For nearly two decades, studies on the distribution of the field-aligned current have been very active and also controversial regarding the topology of the dayside field-aligned currents. Two types of field-aligned current patterns have been proposed: (1) the cusp/mantle currents are topologically separated from the region 1 currents [*Iijima and Potemra*, 1976; *Potemra et al.*, 1980; *Troshichev*, 1982; *Burch et al.*, 1985; *Erlandson et al.*, 1988; *Friis-Christensen and Lassen*, 1991; *Taguchi et al.*, 1993]; (2) the cusp/mantle currents are an extension of the region 1 currents from either dawn or dusk [*McDiarmid et al.*, 1979; *Rich and Maynard*, 1989; *Cowley et al.*, 1991; *Saunders*, 1992; *de la Beaujardiére et al.*, 1993]. On individual satellite passes, it is essentially impossible to distinguish one pattern from another. Although single satellite observations may provide detailed information of spatial structures along the satellite track, it is often difficult to construct the intimate relationship between the different current systems without resorting to assumptions about the structure away from the satellite trajectory.

So far studies on the ionospheric cusp signatures have been conducted through spatially limited observations. It is not only necessary but also critical to extend the cusp study to a global context in order to understand the solar wind-magnetosphere-ionosphere coupling processes. In this paper we attempt to fulfill this goal by constructing the large-scale high-latitude patterns of the ionospheric convection and field-aligned current based on various simultaneous observations both from space and from ground.

2. Procedure and Data Inputs

The assimilative mapping of ionospheric electrodynamics (AMIE) procedure, derived by *Richmond and Kamide* [1988], is applied to derive the large-scale instantaneous patterns of ionospheric conductances, electric fields, currents, and other related quantities by combining simultaneous measurements from satellites, radars, and ground magnetometers. The procedure is an optimally constrained weighted least-squares fit of coefficients to the observed data. Each observation is weighted by the inverse square of its effective error, so that less reliable data contribute less to the fitting. The AMIE procedure also incorporates a priori empirical information about electric potential and ionospheric conductance to improve the estimate in the region where the data coverage is sparse (see *Richmond* [1992] for more details).

In this paper we present some patterns of ionospheric convection and field-aligned current deduced for the period of January 27–29, 1992, which is one of the recent Geospace Environmental Modeling (GEM) observing campaigns. The data which are incorporated into AMIE to derive the global large-scale patterns of electrodynamic fields for this particular GEM period are obtained from (1) satellites; (2) radars; and (3) ground magnetometers. Satellites provided various valuable

data during this period: the IMP 8 satellite monitoring the interplanetary magnetic fields (IMF) and solar wind parameters upstream of the Earth; the four DMSP (F8–F11) satellites measuring the ion drift velocities and the particle precipitations; the NOAA 12 spacecraft observing the precipitating auroral particles. Four radars were also operating simultaneously during this period. They are the Sondrestrom incoherent scatter radar, the European Incoherent Scatter (EISCAT) radar, the Millstone Hill incoherent scatter radar, and the Goose Bay HF radar. The DMSP satellites are in Sun-synchronous circular orbits at an altitude about of 840 km, with orbital inclinations of 98.7° and orbital periods of about 100 min. NOAA 12 is also a polar-orbiting satellite, with an altitude of 850 km and an orbital period of 100 min. All four DMSP satellites measure the cross-track horizontal and vertical ion drift components. Additionally, F10 and F11 can also measure the along-track velocity component. The ion drift measurements are averaged in 20-s segments (about 150 km) and are utilized in the AMIE fitting procedure if they were taken within ±20 min of an analyzed time. The ion drift velocities are converted into electric fields via $\vec{E} = -\vec{v}\times\vec{B}$. The electric fields are then mapped to a reference altitude of 110 km along the geomagnetic field lines. The precipitating electron measurements from the DMSP and NOAA 12 satellites can be used to modify the height-integrated Hall and Pedersen conductances along the satellite track by considering the energy fluxes and average energies of the precipitating electron [*Robinson et al.*, 1987]. The electron data for these calculations were time averaged into 30-s intervals and used only if they were taken within 20 min of the modeling time. A more detailed description of the data has been given by *Lu et al.* [1994]. In addition to the 65 ground magnetometers used in the previous study [*Lu et al.*, 1994], 22 more are added, yielding a total of 87 magnetometer stations; among them 16 stations are from the southern hemisphere. The magnetometer data are averaged to 5-min time resolution. Figures 1a and 1b show the locations of the 83 stations above 40° magnetic latitude in the northern and southern hemispheres, respectively, which are indicated by their international three-letter codes. The AMIE procedure uses apex coordinates [*VanZandt et al.*, 1972]; the apex latitude is very similar to invariant latitude and corrected geomagnetic latitude in the polar regions. All data sets are converted to apex coordinates before incorporation into AMIE. The current grid size of AMIE is about 1.6° in latitude and 10° in longitude.

3. Results

Although there were nearly 300 DMSP passes over the northern and southern polar caps during this 3-day campaign period, the passes which crossed the dayside cusp were still rare due to the inclination of the satellite orbit. The three cases presented below were chosen because not only was the cusp plasma precipitation observed but also the IMF was steady: the signs of the IMF components were unchanged for more than one hour prior to the time when the patterns were derived. Additionally, the AE and AL indices indicate no significant substorm activity corresponding to these patterns. Therefore the patterns should be considered as stable.

3.1. Northern Hemisphere Cases

Figure 2 shows the patterns of the ionospheric convection or electric potential (left panel) and field-aligned current (right panel) in the northern hemisphere derived at 0155 UT of January 29. At this particular

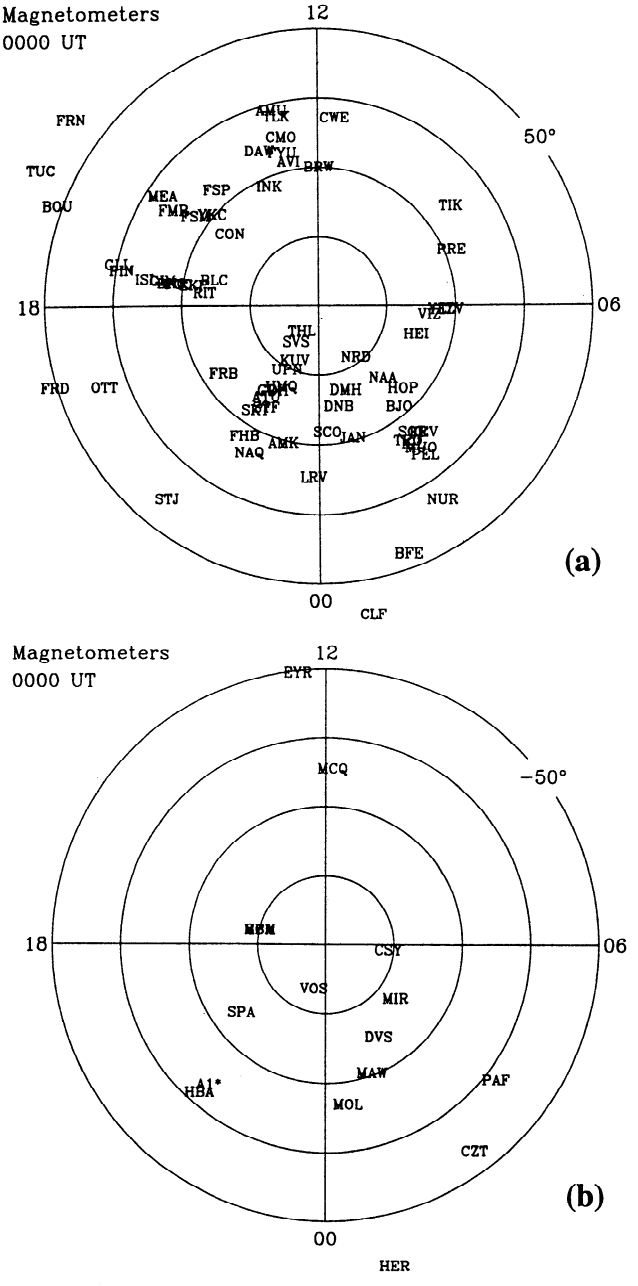

Figure 1. Ground magnetometer locations at 0000 UT in the (a) northern and (b) southern hemispheres, respectively. Only those stations above 40° magnetic latitude, north or south, are shown. The southern hemisphere is viewed as though one were looking through the Earth.

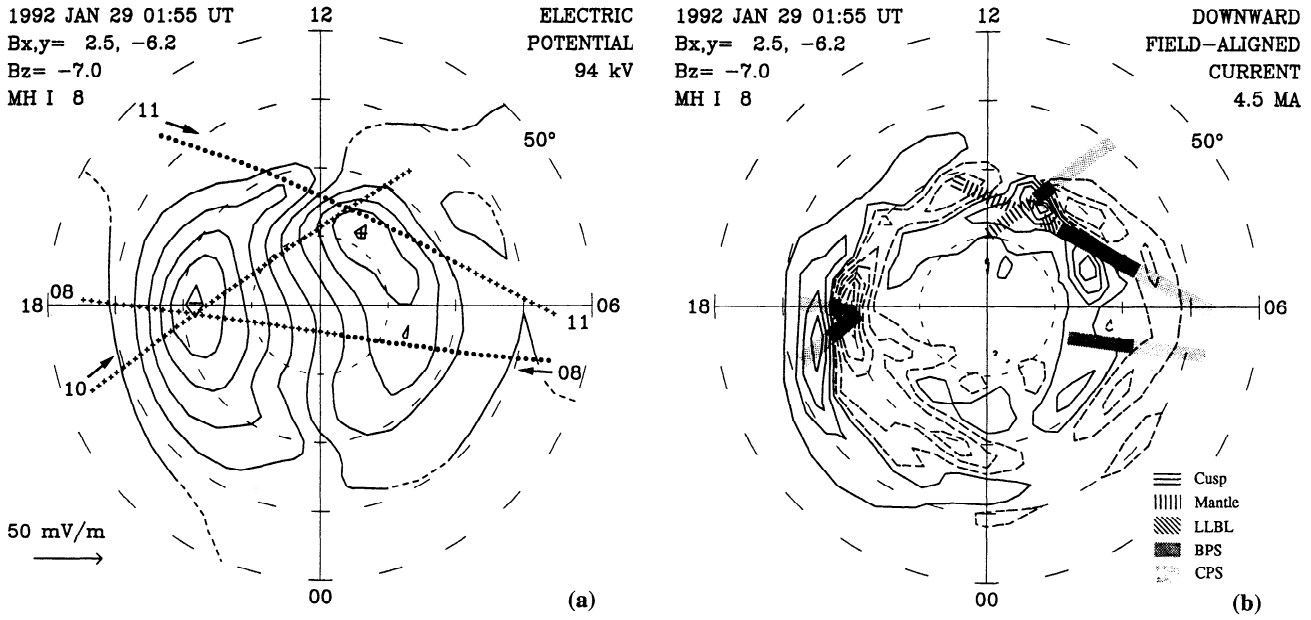

Figure 2. (a) The ionospheric convection pattern derived at 0155 UT on January 29, 1992, in the northern hemisphere. The pattern has a contour interval of 10 kV. The satellite trajectories which have been converted to apex coordinates are indicated as either dots (if the observations were made prior to 0155 UT) or plus signs (if they were made after 0155 UT). The solid arrows show the direction of the satellite motion. (b) Distribution of the field-aligned current density, with solid lines representing the downward current and dashed lines the upward current. The contour interval is 0.3 $\mu A/m^2$, starting at ± 0.1 $\mu A/m^2$. The total downward field-aligned current integrated over the area poleward of 50° latitude is given at the upper right. The different magnetospheric plasma regimes are indicated by the different shadings.

time, the 5-min averaged values of the IMF B_x, B_y, and B_z components in GSM coordinates, given at the upper left of each panel, are 2.5 nT, -6.2 nT, and -7.0 nT, respectively. In Figure 2a, the total cross-polar-cap potential drop is given at the upper right, which is the difference between most positive and most negative potentials. The convection contours are shown as solid lines where the AMIE procedure infers an uncertainty in the large-scale electric field of less than 50%; otherwise the contours are shown as dashed lines. The trajectories of the three DMSP satellites (F8, F10, and F11) are indicated as either dots (if the observations were made prior to the given time at the upper left) or plus signs (if they were made after the given time). The solid arrows show the direction of the satellite motion. The ionospheric convection is predominantly a two-cell pattern, consistent with the southward IMF condition. Enhanced convection flows with speeds exceeding 1000 m/s were measured by the DMSP F11 satellite between 1100 magnetic local time (MLT) and 1300 MLT (between 0148:30 and 0150 UT in Figure 3a). The simultaneous field-aligned current distribution is shown in Figure 2b. Solid contours represents downward field-aligned currents and dashed contours upward currents. The contours have an interval 0.3 $\mu A/m^2$, starting at ± 0.1 $\mu A/m^2$. The total downward field-aligned current integrated over the area poleward of 50° latitude is 4.5 MA, given at the upper right. The general features illustrated here are similar to the statistical patterns of *Iijima and Potemra* [1976]: on the dawnside the region 1 current is downward and region 2 current is upward; on the duskside, the region 1 current is upward and region 2 current is downward. Near local noon, the morning side downward current expands into the afternoon sector and overlaps with the upward current between 1200 and 1700 MLT. Along with the region 2 current from the duskside, they form a triple current sheet. For negative B_y, as in this case, the downward current is located poleward of the upward current.

The corresponding energy spectrograms of the precipitating particles measured by DMSP F8, F10, and F11 are shown in Plates 1, 2, and 3, respectively. On these spectrograms we note the ionospheric projections of various magnetospheric plasma source regions, following the DMSP classification [*Newell and Meng*, 1988; *Newell et al.*, 1991a, b]. F8 had an orbit close to the dawn-dusk meridian. It first encountered the central plasma sheet (CPS) and the boundary plasma sheet (BPS) on the dawnside. It then entered the region corresponding to the polar rain (PR) precipitation. The polar rain consists of relatively cold electrons with energies of a few hundred electron volts (eV), which are of solar origin [*Fairfield and Scudder*, 1985]. F8 finally passed through the duskside BPS and CPS. From left to right, Plate 3 shows the energy spectrogram observed when the F11 satellite was moving from postnoon to dawn. On the postnoonside, it encountered a region in which the precipitating ions had a clear energy-latitude dispersion structure. This kind of structure is due to the velocity filter effect [*Shelley et al.*, 1976; *Reiff et*

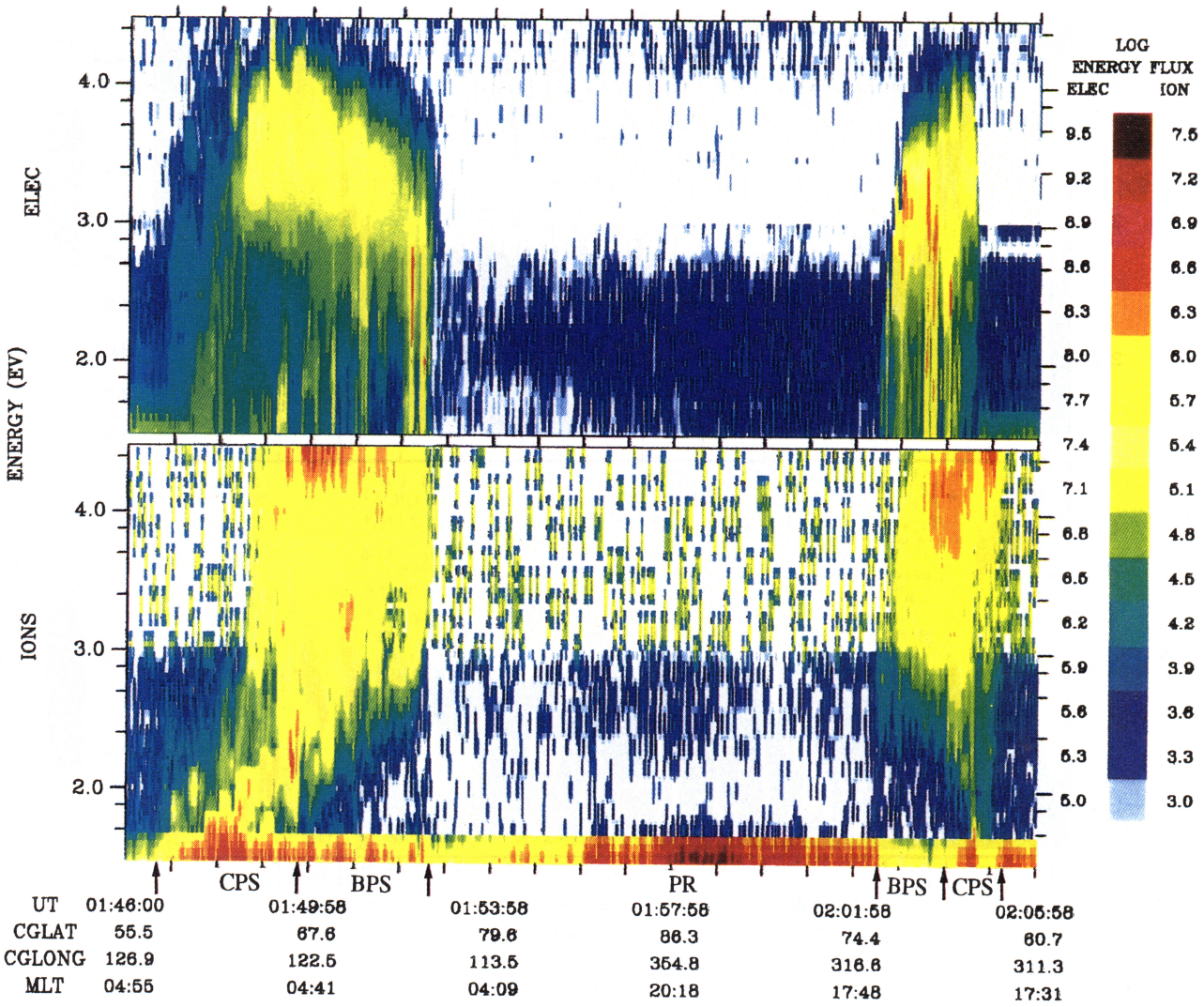

Plate 1. DMSP F8 spectrogram of differential energy flux for 0155 UT on January 29, 1992. The differential energy flux is plotted in units of eV/cm^2 s sr eV, with the precipitating electrons at the top panel and the ions at the bottom panel. The boundaries of different plasma regimes are indicated underneath the spectrogram by the arrows.

al., 1977]. The particle precipitation in this region is well identified as the ionospheric signature of the cusp [*Newell and Meng*, 1988]. Immediately poleward of the cusp is the region called the mantle, which is characterized by less-energetic ions (less than 1 keV) [*Newell et al.*, 1991a]. Next to the mantle is a narrow region filled with polar rain precipitation. F11 then encountered the low-latitude boundary layer (LLBL), the BPS and the CPS on the morning side. Plate 2 is the spectrogram from the DMSP F10. F10 was moving from dusk at about 1800 MLT, across the northern polar cap, towards the dayside. F10 encountered the duskside CPS and BPS, the polar rain, and then the dayside mantle, LLBL, BPS, and CPS. The various precipitating regions observed by the DMSP satellites are indicated by the different shadings in Figure 2b. A more accurate identification of the open-closed field line boundary should be determined from the pitch angle distribution of the energetic (> 30 keV) particles [*Heelis et al.*, 1986; *Coley et al.*, 1987; *Roeder and Lyons*, 1992]. Unfortunately, such data are currently unavailable from the DMSP satellites. In this study we assume that the cusp, mantle, and PR precipitations are on open field lines, and the CPS, BPS, and LLBL on closed field lines. We find that the normal region 1 currents are mainly coincident with the BPS and the region 2 currents coincident with the CPS on both dawnside and duskside. Near local noon, however, the cusp is coincident with the equatorward portion of the upward field-aligned current and the mantle is coincident with downward field-aligned current as well as the poleward portion of the upward current. Further away from noon, the LLBL and BPS

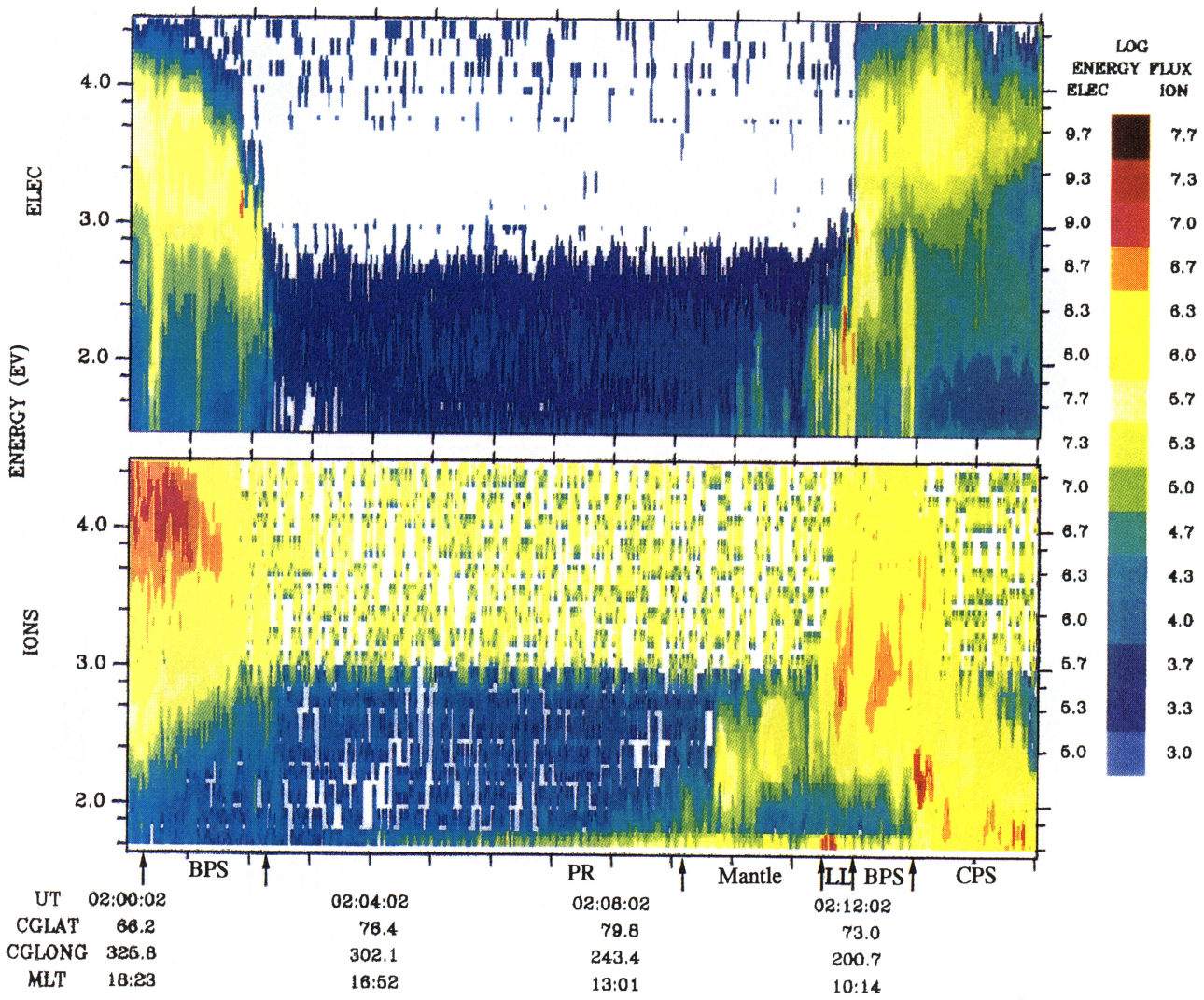

Plate 2. DMSP F10 spectrogram from January 29, 1992, at 0200 UT. The low-latitude boundary layer is labeled as "LL."

are coincident with the morningside downward region 1 current.

While we have presented the large-scale patterns of ionospheric convection and field-aligned current above, we examine in more detail the convection flow in the vicinity of the cusp. Figure 3 shows the ion drift velocity measured by DMSP F11 between 0147 and 0150 UT on January 29. The top panel is the high-resolution (with six samples per second) flow velocity component perpendicular to the satellite track, measured by the Ion Drift Meter (IDM) aboard F11. Positive values correspond to sunward flow and negative values to antisunward flow. The bottom panel shows the 4-s averaged flow component along the satellite track, measured by the F11 retarding potential analyzer (RPA). Positive values indicate that the flow direction is parallel to the trajectory (roughly westward) and negative values indicate antiparallel flow (roughly eastward). Note that the F11 RPA data have large data gaps, and therefore are not incorporated into AMIE to derive the convection pattern. The cusp ion precipitation is identified between 0147:40 and 0148:03 UT. Within this region, Figure 3 shows that the convection flow is sunward and mainly westward. The convection reversal boundary (CRB) is coincident with the poleward boundary of the cusp. Further poleward, within the mantle, the flow becomes strongly antisunward with speeds nearly reaching 3000 m/s.

Figure 4 shows the patterns of ionospheric convection and field-aligned current derived at 0208 UT on January 28, 1992, in the northern hemisphere. The two-cell convection pattern (Figure 4a) is again consistent with the corresponding southward IMF condition. Notice that even though the IMF B_y is more negative (the 5-min averaged value of B_y is -12.5 nT) than in the previous case, the dayside convection flow is not quite

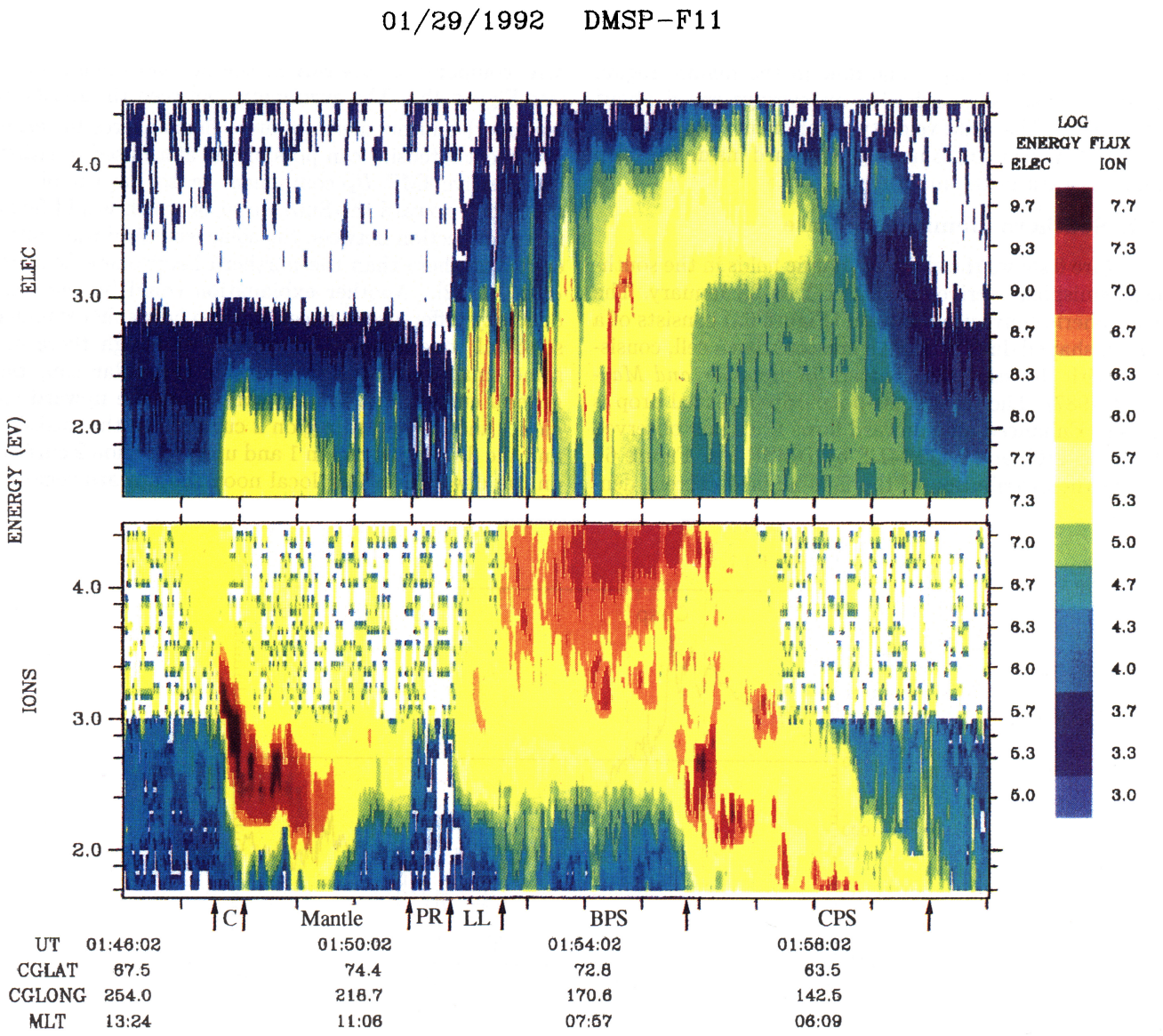

Plate 3. DMSP F11 spectrogram for 0155 UT on January 29, 1992. The cusp is labeled as "C" and the low-latitude boundary layer as "LL."

as eastward as it was in Figure 2a. This is because the dayside convection configuration is determined only by the sunward-antisunward (or the perpendicular-to-track) flow component measured by the F11 IDM. This contrasts with the previous case shown in Figure 2a, in which the nearby DMSP F10 provided ion drift velocities both from IDM and RPA and helped determine the east-west flow in the pattern. This has been confirmed by a "test-run" of the convection pattern without using the F10 data for the previous case. The distribution of field-aligned currents (Figure 4b) consists of two nearly circular current sheets, e.g., the region 1 and region 2 currents. The fact that there is only marginal overlap between the upward region 1 current from the duskside and the downward region 1 current from the dawnside near local noon is caused by the lack of the east-west convection flow in that region as just discussed. The energy spectrograms observed by F8 and F10 (not shown) are very similar to Plates 1 and 3, since the satellite trajectories were very similar to those in the previous case. The different plasma regimes are indicated by the different shadings. Again, the CPS precipitation is coincident with the region 2 current and the BPS is coincident with region 1 currents on both dawn and dusk. Near noon, the cusp is found located at the equatorward edge of the upward region 1 current from dusk, while the mantle corresponds to the downward region 1 current from dawn as well as to the poleward portion of the upward current.

Figure 5, similar to Figure 3, presents the ion drift velocities measured from F11 between 0200 and 0203 UT on January 28, 1992. The cusp is identified between 0200:30 and 0201:10 UT, and is marked between two vertical dashed lines. Within the cusp region, the flow is mainly in the sunward direction, though with some embedded antisunward flow at the poleward part of the

cusp. Again, the CRB (or the most poleward boundary of the sunward flow) is coincident with the poleward boundary of the cusp. The flow in the mantle region is strongly antisunward with an average speed about 1800 m/s. The drift velocity component measured by the RPA instrument is mainly westward inside the cusp and eastward in the mantle.

3.2. Southern Hemisphere Case

Figure 6 shows the electrodynamic fields in the southern hemisphere derived at 0011 UT on 28 January. The ionospheric convection pattern (Figure 6a) consists of a round-shaped dusk cell and a crescent dawn cell, consistent with the statistical pattern of *Heppner and Maynard* [1987]. The total cross-polar-cap potential drop is 85 kV. Enhanced antisunward flows are again observed between 1100 and 1400 MLT by DMSP F9. Figure 6b shows the distribution of the field-aligned current density. The contour interval is 0.4 μA/m^2, starting at $\pm$0.2 μA/m^2. The total downward field-aligned current is 6.3 MA, compared to 4.4 MA in the northern hemisphere (see Figure 4b). The asymmetry between the southern (summer) and northern (winter) hemispheres in terms of current intensity can possibly be attributed to either the positive IMF B_x component or to the tilt of the south pole toward the Sun, either of which would favor more connection between the solar wind and the southern hemisphere than the northern hemisphere [*Zanetti et al.*, 1982]. Another explanation could be the conductivity difference between the two hemispheres under solstitial conditions [*Reiff*, 1982]. Although there are some small-scale structures inside the polar cap, the general current distribution consists of the upward region 1 and downward region 2 currents on the duskside and the downward region 1 and upward region 2 current on the dawnside. Near local noon the upward region 1

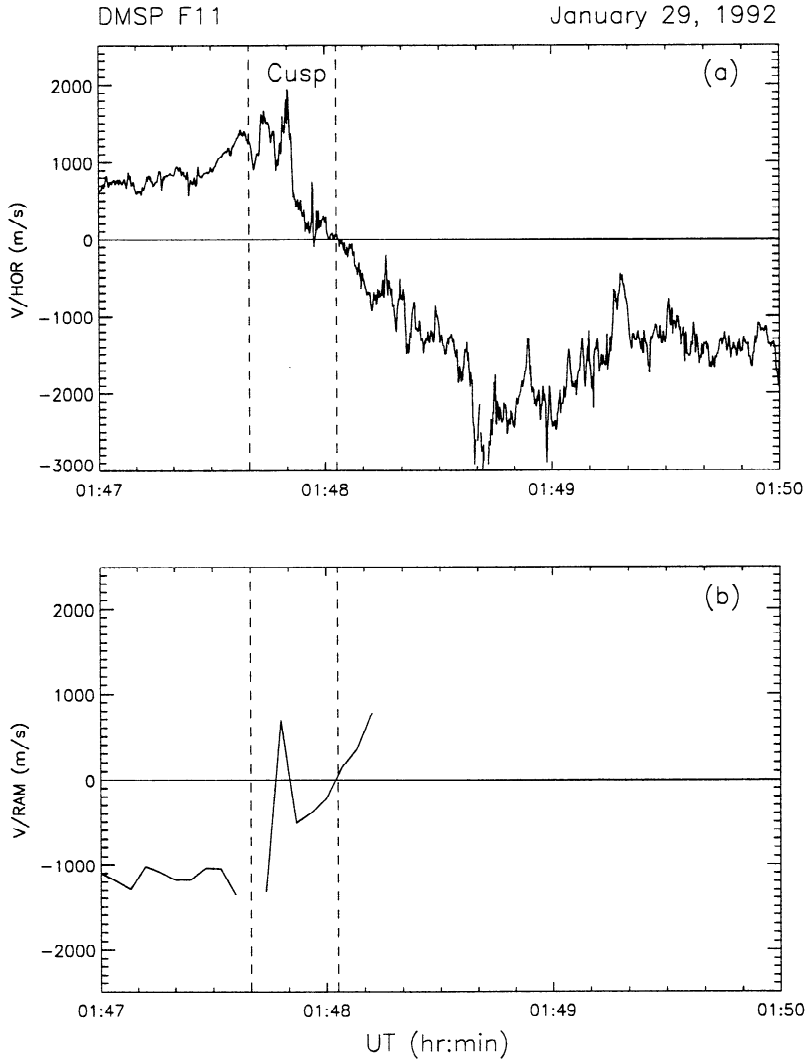

Figure 3. (a) The high-resolution (with 6 samples per second) horizontal flow component perpendicular to the satellite track measured by F11 IDM between 0147 and 0150 UT on January 29, 1992. Positive values correspond to sunward flow and negative values to antisunward flow. The cusp is marked by the vertical dashed lines. (b) The 4-s averaged flow component along the satellite track measured by the F11 RPA. Positive values are for the flow which is parallel to the trajectory (roughly eastward) and negative values for the antiparallel flow (roughly westward).

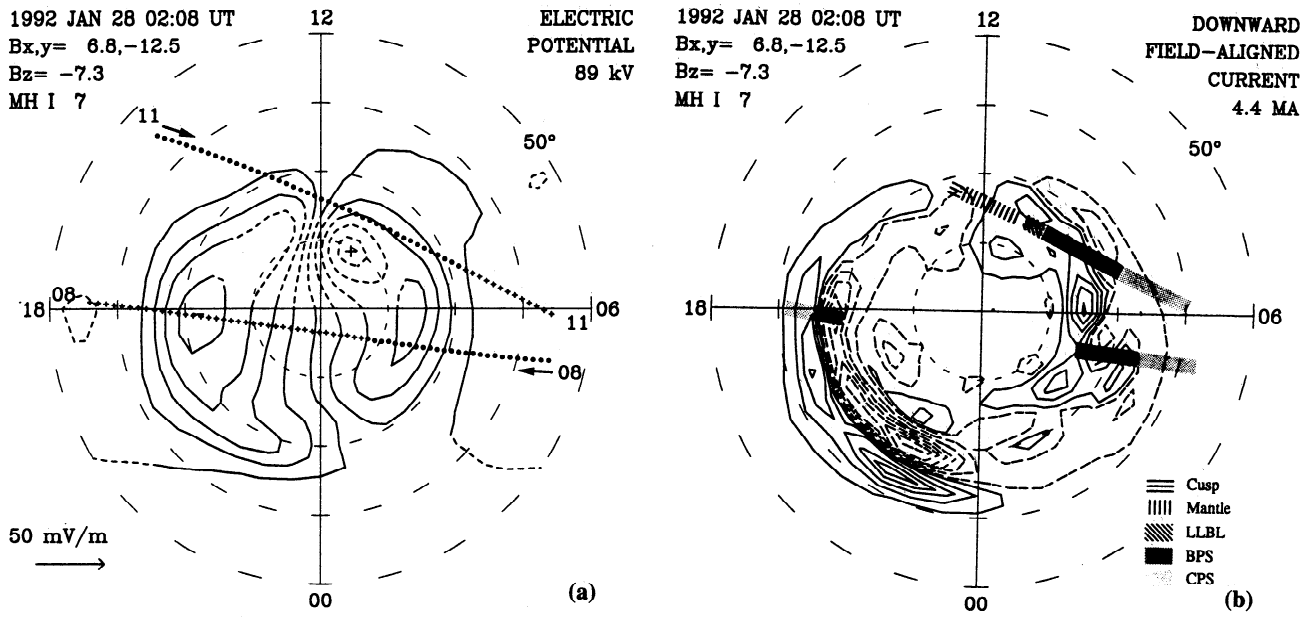

Figure 4. Patterns of the (a) ionospheric convection and (b) field-aligned current derived at 0208 UT on January 28, 1992, in the northern hemisphere.

extends from the duskside slightly into the prenoon sector and overlaps with the region 1 from the morningside between 1100 and 1200 MLT.

By examining the spectrograms of the precipitating particles measured by the DMSP F9 and F10 satellites, the different magnetospheric plasma regions are indicated in Figure 6b. As with the two northern hemisphere cases shown in Figures 2b and 4b, the CPS is colocated with the region 2 currents and the BPS colocated with equatorward part of the region 1 currents near the dawn-dusk meridian. Near noon, a narrow cusp region is found at the equatorward part of the downward region 1 current that extends from the dawnside, and the mantle is found at the poleward part of the downward current as well as the upward region 1 current that extends from dusk.

Figure 7 is the drift component measured by the F9 IDM between 0021 and 0023 UT when F9 was passing over the southern hemisphere. Unfortunately, no RPA instrument was aboard on F9. Again, the drift flow inside the cusp is mainly in the sunward direction, especially at the equatorward edge of the cusp. Note also that there are apparent fluctuations within the cusp. Similar irregular fluctuations are also observed by the EXOS D satellite [*Matsuoka et al.*, 1993] and are attributed to Alfvén waves.

4. Discussion

4.1. Convection Flow Within the Dayside Cusp

It is not uncommon to observe sunward convection flows in the region of open field lines, usually on the dawnside or duskside of the polar cap [*Coley et al.*, 1987; *Nishida et al.*, 1993; *Lu et al.*, 1994]. This phenomenon has been interpreted as a result of the magnetotail lobe field lines merging with the IMF [*Burch et al.*, 1985; *Reiff and Burch*, 1985; *Crooker*, 1992].

As discussed by *Cowley et al.* [1983], the initial motion of the newly merged field lines depends on the force balance between the magnetosheath dragging and magnetic tension. When the IMF has a significant y component, the magnetic tension may overcome the flow dragging so that the newly opened field lines move sunward. Once the field line moves away from the merging site, the magnetic tension gradually relaxes and the flow dragging becomes the dominant force. Then the field lines are dragged tailward. This scenario therefore can explain the sunward flow inside the cusp and antisunward flow in the mantle, as demonstrated in Figures 3, 5, and 7. Sunward flow in the cusp region has also been observed earlier by the Dynamics Explorer satellites in the prenoon sector in the northern (southern) hemisphere for $B_y < 0$ ($B_y > 0$) [*Saflekos et al.*, 1990; *Maynard et al.*, 1991] and is ascribed to the magnetic tension due to the IMF B_y component.

However, our results contradict what models would predict in terms of the location of the cusp. Both theoretical models [*Crooker*, 1979, 1988; *Cowley et al.*, 1991] and statistical models [*Newell et al.*, 1989] show the tendency for the cusp to move toward dawn (dusk) in the northern (southern) hemisphere when B_y is negative. Although it may be due to the particular satellite trajectory, we have found the cusp located postnoon in the northern hemisphere and prenoon in the southern hemisphere. For the case shown in Figure 2, DMSP F11 observed the cusp ion precipitation at about 1300 MLT around 72° magnetic latitude. When the DMSP F10 satellite passed through the dayside polar cap at about 1030 MLT around the same latitude, no cusp signature was found. This seems to indicate that the cusp is spa-

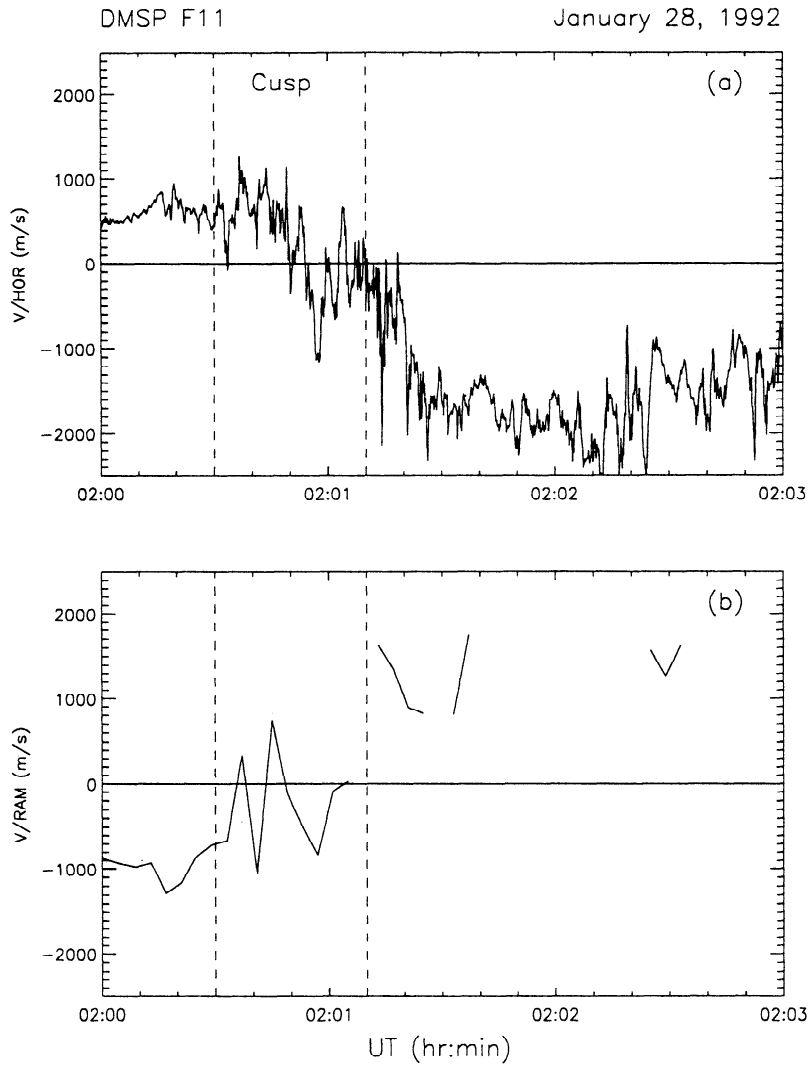

Figure 5. Similar to Figure 3, but measured by F11 between 0200 and 0203 UT on January 28, 1992.

tially confined. A recent statistical survey by *Xu et al.* [1995] also shows that the mantle is more frequently observed in the postnoon sector than in the prenoon sector in the northern hemisphere for $B_y < 0$. Furthermore, for a negative IMF B_y component, the magnetic tension force is expected to be in the same direction as the magnetosheath flow in the dusk (dawn) sector of the northern (southern) hemisphere [e.g., *Cowley et al.*, 1983; *Gosling et al.*, 1990]. Thus the convection flow inside the cusp region should be antisunward rather than sunward on the duskside (dawnside) of the northern (southern) polar cap. However, we note that for a large B_y component, the merging line should have a significant tilt. When $B_y < 0$, the dawnside cusp in the southern hemisphere would result from merging in the northern hemisphere; the duskside cusp in the northern hemisphere would result from merging in the southern hemisphere. For January conditions, the dipole tilt is large and merging in the southern hemisphere should be favored [e.g., *Crooker and Rich*, 1993]. In addition, for the three cases studied, the IMF B_x was positive which also is in favor of merging in the southern hemisphere. Thus the larger fluxes observed on the duskside in the northern hemisphere may result from that effect.

It should also be noted that the cusp, as identified from the DMSP classification, is confined to a rather narrow latitude region (within 2° in latitude). Because of the continuation in the energy spectrogram, it is often difficult to distinguish unambiguously the cusp from the mantle. Using an alternative classification, such as that by *Kremser and Lundin* [1990], one would have a much wider "cusp" by including part of what is otherwise defined as the "mantle" precipitation by *Newell et al.* [1991a]. In such a case, the cusp would then seem to act as a transition zone for the plasma flow from sunward to antisunward.

4.2. Topology of the Dayside Field-Aligned Currents

The relationship between the region 1 and cusp/mantle currents remains an active research subject mainly because of its complication and, sometimes, controversy. Based on DE 2 observations, *Taguchi et al.* [1993] have recently proposed that the cusp/mantle cur-

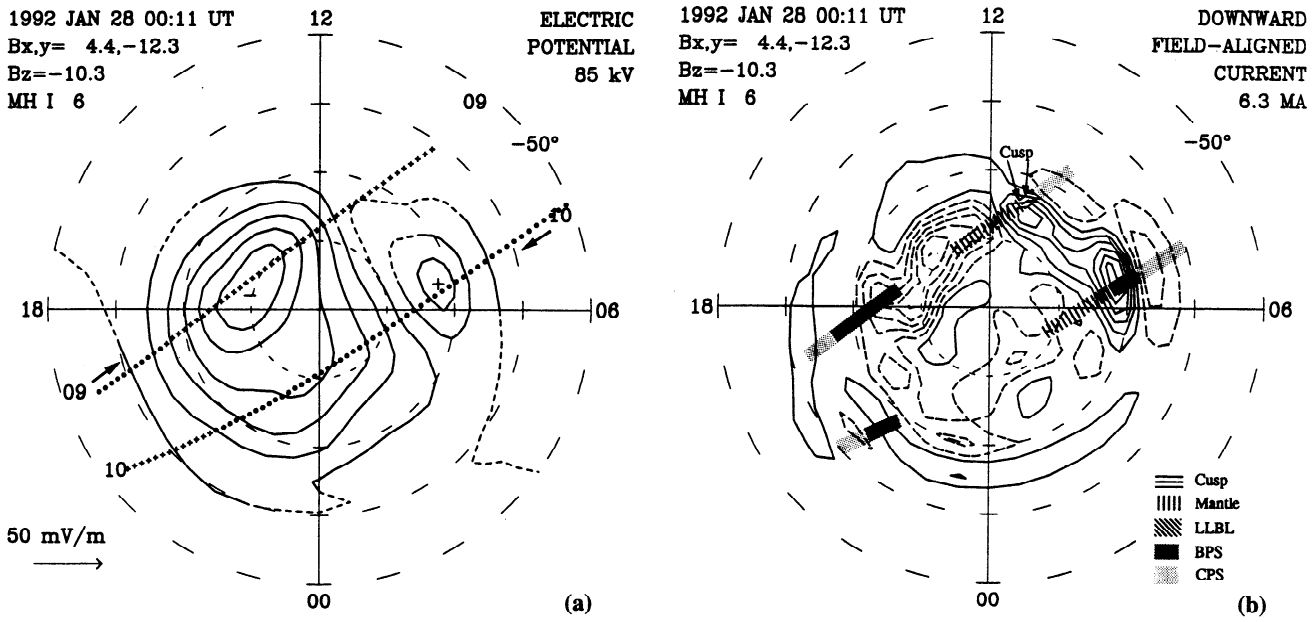

Figure 6. Patterns of the (a) ionospheric convection and (b) field-aligned current derived at 0011 UT on January 28, 1992, in the southern hemisphere. The contour interval for the field-aligned current is 0.4 μA/m^2, starting at $\pm$0.2 μA/m^2.

rents, referred to as the low-latitude cleft current and high-latitude cleft current, are a topologically separate current system and they form a pair of field-aligned currents on open field lines located poleward of the region 1 currents. The polarity of the current pair depends on the sign of the IMF B_y. In contrast, using the combined measurements from the DMSP F7 satellite and from the Sondrestrom radar, *de la Beaujardiére et al.* [1993] suggested that the mantle currents are rather an extension of the region 1 currents. The distributions of the field-aligned currents presented in this paper are based on nearly simultaneous multi-instrument observations both from ground and from space. Therefore, unlike the statistical patterns or single spatially constrained observation, the snapshotlike global distributions derived by AMIE allow us to examine the distinctions between the different field-aligned current systems and the separate magnetospheric processes with which they are associated. AMIE is able to provide unique large-scale two-dimensional distributions of the ionospheric electrodynamic fields by combining various different data sets. Nevertheless, detailed small-scale structures are often smeared out due to the grid size currently adopted by AMIE as well as the spatial resolution of the data coverage.

By comparing the field-aligned current distribution with the corresponding spectrograms of the precipitating particles from the satellites, we are able to map

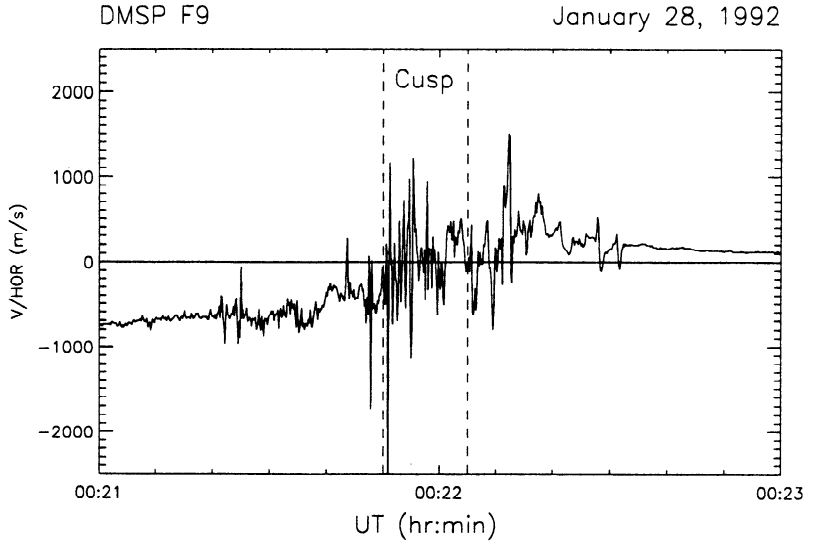

Figure 7. Similar to Figure 3a, but measured by F9 IDM in the southern hemisphere between 0021 UT and 0023 UT on January 28, 1992.

the different magnetospheric plasma regimes into the ionosphere. Near the dawn-dusk meridian, the CPS precipitation is coincident with the region 2 currents. The region 1 currents are located mainly within the region of BPS precipitation as well as expanding poleward into the region of polar rain or mantle precipitation. Near local noon, on the other hand, triple current sheets are often observed. The most equatorward current sheet appears as the extension of the region 2 current from the duskside (dawnside) in the northern (southern) hemisphere and is coincident with ring current or CPS plasma precipitation which originates in the closed magnetic field region. When the IMF B_y is negative, the two poleward sheets form a pair of currents with opposite polarity, e.g., upward current at lower latitudes and downward at higher latitudes in the northern hemisphere. In the southern hemisphere, the polarity of the currents is opposite to that in the northern hemisphere. The cusps are found in the equatorward portion of the upward (downward) current at lower latitudes, and the mantle plasmas are colocated with the downward (upward) current at higher latitudes as well as the poleward portion of the upward (downward) current in the northern (southern) hemisphere. It is therefore evident that the pair of currents near noon, i.e., the cusp/mantle currents, map to the different magnetospheric regimes from those where the normal dawn and dusk region 1 currents map to. This implies that the cusp/mantle and region 1 currents are generated through different mechanisms and therefore should be considered as different current systems.

On the other hand, the patterns of the field-aligned current presented in Figures 2b, 4b, and 6b show clearly the relationship between the cusp/mantle current and the region 1 current, that is, the cusp/mantle currents are apparently topologically connected with the region 1 currents from both dawnside and duskside. In this respect, the cusp/mantle and the region 1 currents may be considered as one current system.

Much modeling effort has been made to interpret the formation of the dayside field-aligned currents. Some models suggest that the cusp currents are derived from the magnetopause currents which shield out the IMF from the magnetosphere [e.g., *Primdahl and Spangslev*, 1981; *Barbosa*, 1984]. Others propose that the field line kinks at the magnetopause are the cause of the cusp currents [e.g., *Saunders*, 1992]. Recent models have focused on the ionosphere as a source of the field-aligned currents [*Mei et al.*, 1994]. By applying an expanding polar cap model with the solar wind electric field only mapping to a confined area in the vicinity of the cusp, *Mei et al.* [1994] provide a synthesis view of the field-aligned currents. In their model, the currents bordering the the cusp (or the cusp currents) are directly driven by the solar wind electric field; the normal region 1 currents around the rest of the polar cap boundary result from the ionospheric response to the applied electric field. Together they form the overlapping pattern in the cusp region.

It is worth pointing out that the patterns of the field-aligned currents presented in this paper are derived indirectly from the electric fields and conductances through Ohm's law. Because of incompleteness of the data coverage, small-scale structures of the field-aligned currents tend to be smeared out by the AMIE procedure. Additionally, there were no satellite magnetometer data available for this period. Therefore the field-aligned currents presented in this paper should be used with caution in terms of their magnitudes and boundaries.

4.3. Location of the Dayside Separatrix

The magnetic merging processes at the dayside magnetopause could be either quasi-steady state [*Crooker*, 1988; *Cowley et al.*, 1991] or impulsive, such as the flux transfer events (FTEs) with an average recurrence period of 8 min [*Rijnbeek et al.*, 1984]. For a steady-state process, the newly opened magnetic field lines would propagate tailward with the same velocity as the plasma convection; whereas, for an FTE, the new magnetic flux tube would move across the polar cap with respect to the background plasma flow. Although flux transfer events are commonly observed [*Russell and Elphic*, 1979; *Rijnbeek et al.*, 1984; *Lockwood and Smith*, 1989; *Lockwood et al.*, 1990], a serious argument is raised regarding the contribution of the FTE to the total cross-polar-cap potential drop [*Cowley*, 1984; *Denig et al.*, 1993; *Newell and Sibeck*, 1993]. In this study, we assume that the merging process is quasi-steady state, rather than try to distinguish one process from the other. The particle spectrograms of the DMSP satellites (see Plate 3) show smooth and continuous dispersion structure within the cusp region, which supports our assumption of quasi-steady state merging processes.

In the ionosphere, the separatrix marks the boundary between open and closed magnetic field lines. The dayside separatrix maps along the field lines from the ionosphere to the dayside merging line or X line on the magnetopause. To estimate the location of the dayside separatrix in the ionosphere, we assume that the merging occurs along the dayside magnetopause where the newly opened field lines all have the same length L between the merging site and the ionospheric footprint. Note that such assumption is true only in the vicinity of local noon. The highest-energy magnetosheath particles are located at the equatorward boundary of the cusp in the ionosphere, while the lower-energy particles appear to be shifted further poleward, which forms the typical energy-latitude dispersion structure in the dayside cusp region. We consider here only the ions which have zero pitch angle and precipitate adiabatically into the ionosphere along the field lines. The same approximation has been made in previous studies [*Shelley et al.*, 1976; *Reiff et al.*, 1977; *Menietti and Burch*, 1988; *Lockwood and Smith*, 1992]. For an energetic ion with energy E and mass M, the travel time from the merging site at the magnetopause to the ionosphere is $t = L/(2E/M)^{1/2}$. For a less energetic ion with energy E' the travel time is $t' = L/(2E'/M)^{1/2}$. For magnetosheath ions, M can be taken as the proton mass. The

corresponding ionospheric traveling distance d can be written as:

$$d = V_c \times (t' - t) = V_c \times \left(\frac{L}{\sqrt{2E'/M}} - \frac{L}{\sqrt{2E/M}} \right) \quad (1)$$

where V_c is the convection flow speed in the ionosphere. Therefore from (1), we can estimate the length of the field line from the magnetopause to the ionosphere:

$$L = \frac{d}{V_c \times \left(\sqrt{M/2E'} - \sqrt{M/2E} \right)} \quad (2)$$

In the case of the DMSP F11 pass around 0155 UT on January 29, the ion energy E associated with the peak energy flux at the equatorward boundary of the cusp is about 1.4 keV. At the poleward boundary of the cusp, we have chosen a "cutoff" ion energy E' of 125 eV which corresponds to the ion energy flux about 10% of its peak value as determined from the energy spectrum. This choice is somewhat arbitrary and is made to estimate the lower limit of L, as adopted by *Lockwood and Smith* [1992]. The ions with cutoff energy observed in the ionosphere at any given latitude represent the particles that have originated from nearest the merging site [*Onsager et al.*, 1993]. The width of the cusp crossed by the satellite is about 210 km. From Figure 8a, the average convection speed V_c parallel to the satellite track within the cusp is estimated to be 550 m/s, which is consistent with the average drift speed measured by the F11 RPA instrument shown in Figure 3b. Substituting these values into (2), we then estimate the lower limit of L to be about 15 R_E. Once L is determined, we can estimate the relative distance between the ionospheric footprint of the separatrix and the observation point along the satellite orbit by using (1). We assume that the magnetosheath source distribution has the same characteristics so that the "characteristic" ion energy E corresponding to the peak energy flux, E = 1.4 keV in this case, does not change along the dayside magnetopause. The "cutoff" energy E' where the ion energy flux falls to 10% of the peak value is determined from the individual energy spectrum of the precipitating ions at each observation point. The arrows in Figure 8a represent the convection velocities along the satellite trajectory, with a scale vector given at the lower left. Since only the cross-track velocity (or along-track electric field) component from F11 was used, the other vector component shown in the plot is actually derived from the AMIE fitting procedure. Note that the magnetosheath flow speed increases during propagation away from the merging site toward the tail. In the ionosphere, the convection patterns (e.g., Figures 2a, 4a, and 6a) show that the flows converge from lower latitude to higher latitude near local noon. For this reason, we have chosen the effective convection speed $V_c = \frac{2}{3}V$. We then estimate the location of the separatrix mapping to the ionosphere, which is indicated by the open circles in Figure 8a. The cross signs, on the other hand, show the open-closed boundary obtained directly from the energy spectrograms. It

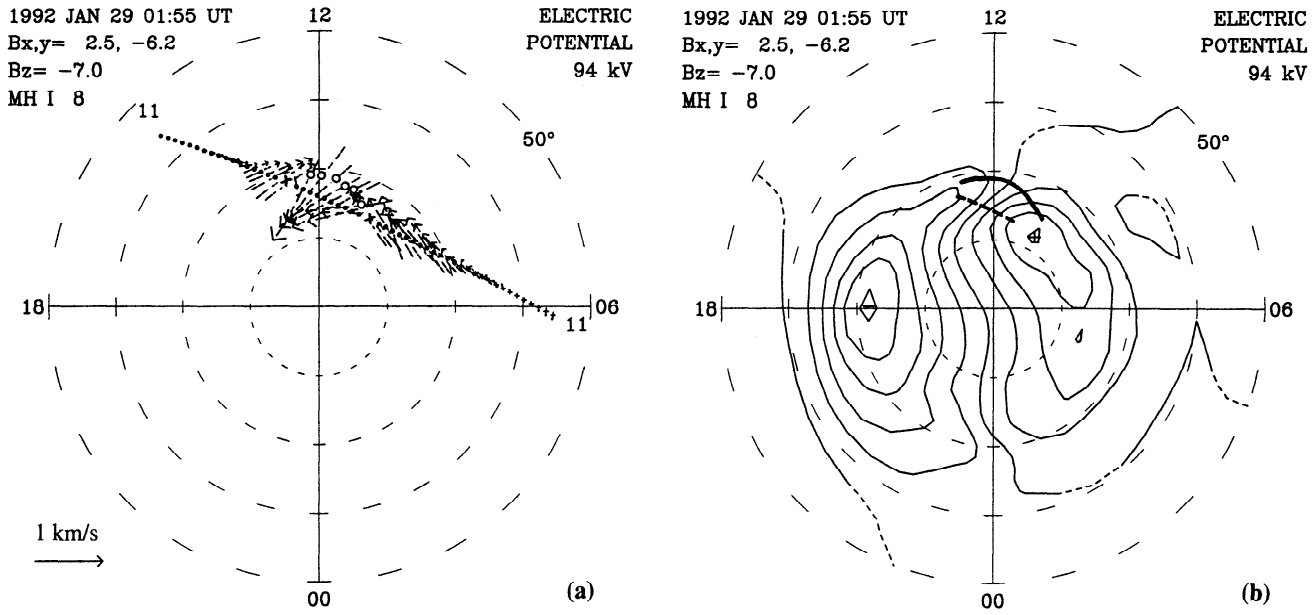

Figure 8. (a) The dashed arrows indicate the convection velocities along the DMSP F11 trajectory at about 0155 UT on January 29, 1992. Note that only the cross-track velocity (or along-track electric field) component was incorporated into AMIE, the other vector component shown in the plot is actually derived from the AMIE fitting procedure. The open circles show the location of the estimated separatrix. The cross signs indicate the open-closed field line boundary from the energy spectrogram. (b) The ionospheric convection pattern derived at 0155 UT, with the separatrix indicated by the heavy solid line and the throat by the heavy dashed line.

is interesting to note that the open circle is coincident with the cross sign which is the boundary between the mantle and the LLBL observed by F10 at about 73° latitude near 1100 MLT. It therefore implies that the assumptions made above to estimate the separatrix are reasonable. By smoothly connecting the open circles and the plus signs, the dayside separatrix is indicated by the heavy solid line in Figure 8b. As a comparison, the heavy dashed line indicates the "throat" where the convection flow converges [*Heelis et al.*, 1976]. Thus the throat is located about 5° in latitude poleward of the separatrix. In some previous studies [e.g., *Heelis et al.*, 1983; *Reiff and Burch*, 1985; *Siscoe and Huang*, 1985; *Moses et al.*, 1987], the throat has been taken as the location of the separatrix. We would like to point out that, although the effective velocity V_c is arbitrarily chosen to be $\frac{2}{3}V$, it in fact represents approximately the average flow velocity in the region between the separatrix (the heavy solid line) and the satellite track (about the same location as the heavy dashed line) in Figure 8b. If we choose $V_c = V$ instead, the separatrix would be moved about 1° to 2° equatorward. However, such displacement is not significant, comparing with the grid size of AMIE.

Once we know the location of the separatrix as well as the electric potential drop along this line, we are able to estimate the reconnection rate by using the following equation:

$$B_0\, l\, \frac{dx}{dt} = \Phi \qquad (3)$$

where B_0 is the magnetic field strength in the cusp region, l is the length of the separatrix, dx/dt is the reconnection velocity mapped to the ionosphere at which open flux moves across the separatrix, and Φ is the potential drop along l. From Figure 8b, we estimate that Φ is about 47 kV and l is about 1700 km. Thus the reconnection velocity dx/dt is about 550 m/s.

The same procedure is also applied to the case at 0208 UT on January 28, 1992. Figure 9 shows the location of the separatrix. In this case, Φ is about 36 kV and l is 1800 km. From (3), we then estimate the reconnection velocity to be about 400 m/s. Our estimated reconnection velocities are consistent with those measurements (between 300 and 800 m/s) by *de la Beaujardiére et al.* [1991].

We should emphasize here that the assumptions made above to estimate the location of the separatrix and the reconnection velocity are not always valid. For instance, the length of the field line between the merging site and the ionospheric footprint should increase further away from local noon according to any generally accepted magnetic field models. Note that the latitude of the estimated separatrix increases rapidly from about 1100 to 1000 MLT in the Figures 8 and 9. This may be an artifact of the assumption of constant field line length. For the case of Figure 9, if one increases the length L from 15 R_E to 20 R_E, the separatrix would be located about 2° equatorward of the position shown.

5. Summary

We have presented in this paper the large-scale high-latitude ionospheric convection patterns and the field-aligned current distributions based on the extensive data obtained simultaneously both from ground and from space. By comparing these patterns with the corresponding satellite energy spectrograms of the precipitating particles, we are able to examine the the relation of the plasma convection and field-aligned current to the different magnetospheric plasma regimes. It was found that the convection inside the cusp in both northern

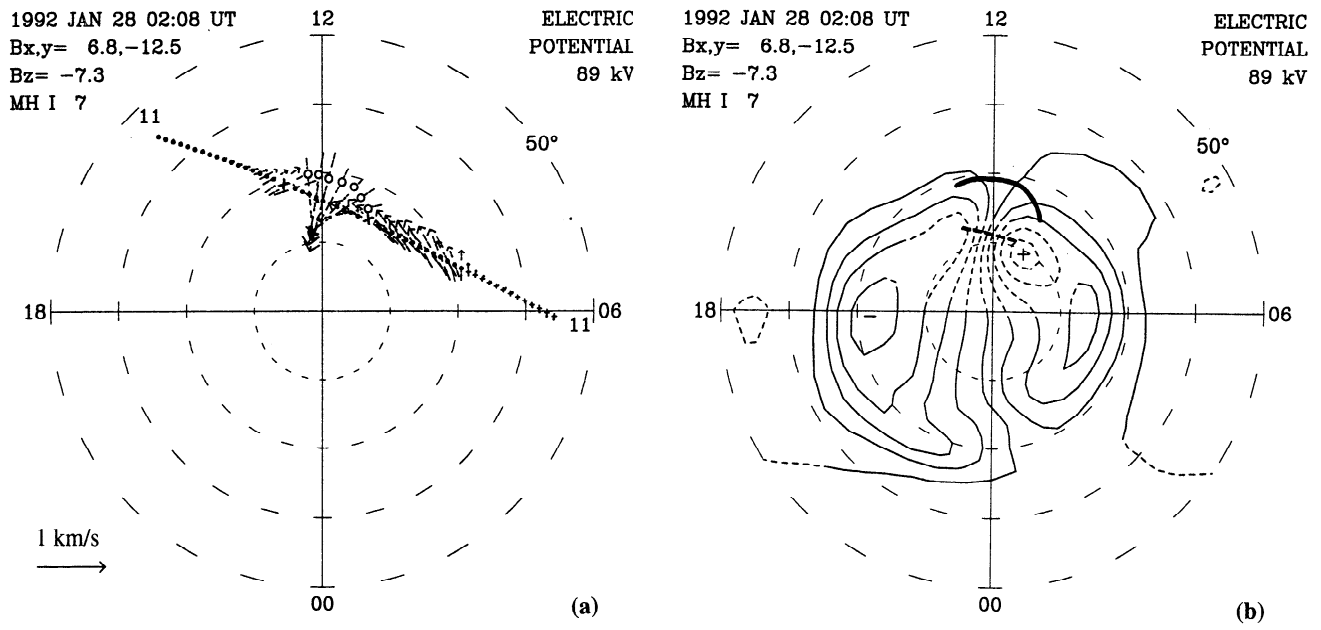

Figure 9. Similar to Figure 8, but for the case at 0011 UT on January 28, 1992.

and southern hemispheres had a more sunward than antisunward component. This cannot be simply explained by the effect of the IMF B_y component (B_y was negative in this study) which would otherwise lead us to expect an antisunward rather than sunward motion in the duskside (dawnside) cusp of the northern (southern) hemisphere. We suggest that this difference may be caused by the fact that northern hemisphere is in winter and merging in the southern hemisphere is favored. This may cause more precipitating flux on the duskside than on the dawnside in the northern hemisphere when $B_y < 0$. Unfortunately, we did not have a spacecraft passing through the duskside southern hemisphere cusp region to test that hypothesis. In this study, we have assumed that the cusp and mantle are on open field lines and the BPS and CPS are on closed field lines. Examination of the precipitating particles reveals that the field-aligned currents near local noon, i.e., the cusp/mantle currents, are associated with the cusp and mantle plasmas which therefore are on open field lines. In contrast, the dawnside and duskside normal region 1 currents are mainly coincident with the plasma sheet particle precipitation along closed field lines. It then implies that the cusp/mantle currents are generated through different mechanisms from the region 1 currents. On the other hand, the patterns of the field-aligned current show clearly the topological connection between the cusp/mantle currents and the region 1 currents. In this respect they may be considered as one current system. Under the assumption of quasi-steady state reconnection, we have also estimated the location of the separatrix in the ionosphere and the reconnection velocity which is between 400 to 550 m/s. It is also clear that, for the two cases examined, the separatrix lies equatorward of the dayside convection throat.

Acknowledgments. We wish to acknowledge the Coupling, Energetics and Dynamics of Atmospheric Regions (CEDAR) Data Base at the National Center for Atmospheric Research (NCAR) for providing the Sondrestrom and Millstone Hill incoherent scatter radar data. All the above facilities are supported by the National Science Foundation (NSF). Johns Hopkins University Applied Physics Laboratory HF radar at Goose Bay, Labrador, is supported in part by the NSF Division of Atmospheric Sciences under NSF grant ATM-9003860 and in part by the National Aeronautics and Space Administration (NASA) under grant NAG5-1099. The EISCAT Scientific Association is supported by the CNRS of France, the SA of Finland, the MPG of Germany, the NAVF of Norway, the NFR of Sweden, and the SERC of Great Britain. The IMAGE magnetometer network is supported by the Finnish Meteorological Institute. We thank L. Morris at the World Data Center for selecting the ground magnetometer data, the Canadian Space Agency and T. Hughes at the National Research Council of Canada for providing data from the CANOPUS magnetometer array, the Auroral Observatory at the University of Tromso, Norway for contributing data from the Norwagian Arctic Stations, O. Troshichev at the Arctic and Antarctic Research Institute for supplying the Russian Arctic and Antarctic magnetogram analog data, P. Sutcliffe at the Hermanus Magnetic Observatory in South Africa for submitting the Hermanus magnetometer data, A. Rodger at the British Antarctic Survey for helping obtaining the Halley and A77 magnetometer data, and D. Singh and D. Neudegg at the Australian Antarctic Division for the collection of the data at Casey and Davis stations in 1992. We also wish to thank C. G. Maclennan and L. J. Lanzerotti of AT&T Bell Laboratories for providing data from their ground stations at Iqaluit (FRB) in Canada, and at McMurdo (MCM) and South Pole (SPA) in the Antarctic. The magnetometer installation at Iqaluit is partially supported by grant DPP-89-21094 to Allan Wolfe of NYCTC from Division of Polar Programs of the NSF. The IMP-8 IMF data was kindly provided by R. Lepping at NASA Goddard Space Flight Center. The Dst index was provided by T. Kamei of the World Data Center C2 at Kyoto University and by M. Sugiura of Tokai University in Japan. We are indebted to T. Wilson at the National Geophysical Data Center for preparing the DMSP particle spectrograms, D. Evans and M. Codrescu at SEL/NOAA for providing NOAA 12 particle data, and B. Emery of the High Altitude Observatory (HAO) at NCAR for assistance in analyzing the ground magnetometer data. We are also grateful to A. Richmond and P. Song at HAO/NCAR for many helpful comments and for carefully reading the manuscript. L. Lyons was supported by NSF grant ATM91-20072. P. Reiff was supported in part by NSF grant ATM-9103440 and NASA grant NAGW-1655. O. de la Beaujardiére was supported by NSF grant 9202795. W. Denig and F. Rich were supported by the Air Force Office of Scientific Research Task PL013. M. Persson was supported by the Swedish Natural Science Research Council (NFR). A. McEwin publishes with permission of the Executive Director of the Australian Geological Survey. The National Center for Atmospheric Research is sponsored by the National Science Foundation.

The Editor thanks D. J. Knudsen and T. J. Rosenberg for their assistance in evaluating this paper.

References

Barbosa, D. D., Dynamics of field-aligned current sources at Earth and Jupiter, in *Magnetospheric Currents, Geophys. Monogr. Ser.*, vol. 28, edited by T. A. Potemra, p. 350, AGU, Washington, D. C., 1984.

Burch, J. L., P. H. Reiff, J. D. Menietti, R. A. Heelis, W. B. Hanson, S. D. Shawhan, E. G. Shelley, M. Sugiura, D. R. Weimer, and J. D. Winningham, IMF B_y-dependent plasma flow and Birkeland currents in the dayside magnetosphere, 1, Dynamics Explorer observations, *J. Geophys. Res.*, *90*, 1577, 1985.

Bythrow, P. F., T. A. Potemra, R. E. Erlandson, L. J. Zanetti, and D. M. Klumpar, Birkeland currents and charged particles in the high-latitude prenoon region: A new interpretation, *J. Geophys. Res.*, *93*, 9791, 1988.

Coley, W. R., R. A. Heelis, W. B. Hanson, P. H. Reiff, J. R. Sharber, and J. D. Winningham, Ionospheric convection signatures and magnetic field topology, *J. Geophys. Res.*, *92*, 12,352, 1987.

Cowley, S. W. H., Solar wind control of magnetospheric convection, Proceedings of the Conference on Achievements of the IMS, *Eur. Space Agency Spec. Publ.*, *217*, 483, 1984.

Cowley, S. W. H., D. J. Southwood, and M. A. Saunders, Interpretation of magnetic field perturbations in the Earth's magnetopause boundary layers, *Planet. Space Sci.*, *31*, 1237, 1983.

Cowley, S. W. H., J. P. Morelli, and M. Lockwood, Dependence of convection flows and particle precipitation in the high-latitude dayside ionosphere on the X and Y components of the interplanetary magnetic field, *J. Geophys. Res.*, *96*, 5557, 1991.

Crooker, N. U., Dayside merging and cusp geometry, *J. Geophys. Res.*, *84*, 951, 1979.

Crooker, N. U., Mapping the merging potential from the magnetopause to the ionosphere through the dayside cusp, *J. Geophys. Res.*, *93*, 7338, 1988.

Crooker, N. U., Reverse convection, *J. Geophys. Res.*, *97*, 19,363, 1992.

Crooker, N. U., and F. J. Rich, Lobe-cell convection as a summer phenomenon, *J. Geophys. Res.*, *98*, 13,403, 1993.

de la Beaujardiére, O., L. R. Lyons, and E. Friis-Christensen, Sondrestrom radar measurements of the reconnection electric field, *J. Geophys. Res.*, *96*, 13,907, 1991.

de la Beaujardiére, O., J. Watermann, P. T. Newell, and F. J. Rich, Relationship between Birkeland current regions, particle precipitation, and electric fields, *J. Geophys. Res.*, *98*, 7711, 1993.

Denig, W. F., et al., Ionospheric signatures of dayside magnetopause transients: A case study using satellite and ground measurements, *J. Geophys. Res.*, *98*, 5969, 1993.

Erlandson, R. E., L. J. Zanetti, T. A. Potemra, and P. F. Bythrow, IMF B_y dependence of region 1 Birkeland currents near noon, *J. Geophys. Res.*, *93*, 9804, 1988.

Fairfield, D. H., and J. D. Scudder, Polar rain: Solar coronal electrons in the Earth's magnetosphere, *J. Geophys. Res.*, *90*, 4055, 1985.

Friis-Christensen, E., and K. Lassen, Large-scale distribution of discrete auroras and field-aligned current, in *Auroral Physics*, edited by C.-I. Meng, M. Rycroft, and L. A. Frank, p. 369, Cambridge University Press, New York, 1991.

Gosling, J. T., M. F. Thomsen, S. J. Bame, R. C. Elphic, C. T. Russell, Plasma flow reversals at the dayside magnetopause and the origin of asymmetric polar cap convection, *J. Geophys. Res.*, *95*, 8073, 1990.

Greenwald, R. A., K. B. Baker, J. M. Ruohoniemi, J. R. Dudeney, M. Pinnrock, N. Mattin, L. M. Leonard, and R. P. Lepping, Simultaneous conjugate observations of dynamic variations in high-latitude dayside convection due to changes in IMF B_y, *J. Geophys. Res.*, *95*, 8057, 1990.

Heelis, R. A., The effects of interplanetary magnetic field orientation on the dayside high-latitude convection, *J. Geophys. Res.*, *89*, 2880, 1984.

Heelis, R. A., W. B. Hanson, and J. L. Burch, Ion convection velocity reversals in the dayside cleft, *J. Geophys. Res.*, *81*, 3803, 1976.

Heelis, R. A., J. C. Foster, O. de la Beaujardiére, and J. Holt, Multistation measurements of high-latitude ionospheric convection, *J. Geophys. Res.*, *88*, 10,111, 1983.

Heelis, R. A., P. H. Reiff, J. D. Winningham, and W. B. Hanson, Ionospheric convection signatures observed by DE 2 during northward interplanetary magnetic field, *J. Geophys. Res.*, *91*, 5817, 1986.

Heppner, J. P., and N. C. Maynard, Empirical high-latitude electric field models, *J. Geophys. Res.*, *92*, 4467, 1987.

Iijima, T., and T. A. Potemra, Field-aligned currents in the dayside cusp observed by Triad, *J. Geophys. Res.*, *81*, 5971, 1976.

Kremser, G., and R. Lundin, Average spatial distributions of energetic particles in the midaltitude cusp/cleft region observed by Viking, *J. Geophys. Res.*, *95*, 5753, 1990.

Lockwood, M., and M. F. Smith, Low-altitude signatures of the cusp and flux transfer events, *Geophys. Res. Lett.*, *16*, 879, 1989.

Lockwood, M., and M. F. Smith, The variation of reconnection rate at the dayside magnetopause and cusp ion precipitation, *J. Geophys. Res.*, *97*, 14,841, 1992.

Lockwood, M., S. W. H. Cowley, P. E. Sandholt, and R. P. Lepping, The ionospheric signatures of flux transfer events and solar wind dynamic pressure changes, *J. Geophys. Res.*, *95*, 17,113, 1990.

Lu, G., et al., Interhemispheric asymmetry of the high-latitude ionospheric convection pattern, *J. Geophys. Res.*, *99*, 6491, 1994.

Lundin, R., On the magnetospheric boundary layer and solar wind energy transfer into the magnetosphere, *Space Sci. Rev.*, *48*, 263, 1988.

Maynard, N. C., T. L. Aggson, E. M. Basinska, W. J. Burke, P. Craven, W. K. Peterson, M. Sugiura, and D. R. Weimer, Magnetospheric boundary dynamics: DE 1 and DE 2 observations near the magnetopause and cusp, *J. Geophys. Res.*, *96*, 3505, 1991.

Matsuoka, A., K. Tsuruda, H. Hayakawa, T. Maukai, A. Nishida, T. Okada, N. Kaya, and H. Fukunishi, Electric field fluctuations and charged particle precipitation in the cusp, *J. Geophys. Res.*, *98*, 11,225, 1993.

McDiarmid, I. B., J. R. Burrows, and M. D. Wilson, Large-scale magnetic field perturbations and particle measurements at 1400 km on the dayside, *J. Geophys. Res.*, *84*, 1431, 1979.

Mei, Y., N. U. Crooker, and G. L. Siscoe, Cusp current modeling: A systematic approach, *J. Geophys. Res.*, *99*, 4027, 1994.

Menietti, J. D., and J. L. Burch, Spatial extent of the plasma injection region in the cusp-magnetosheath interface, *J. Geophys. Res.*, *93*, 105, 1988.

Moses, J. J., G. L. Siscoe, N. U. Crooker, and D. J. Gorney, IMF B_y and day-night conductivity effects in the expanding polar cap convection model, *J. Geophys. Res.*, *92*, 1193, 1987.

Newell, P. T., and C. -I. Meng, The cusp and the cleft/LLBL: Low altitude identification and statistical local time variation, *J. Geophys. Res.*, *93*, 14,549, 1988.

Newell, P. T., and D. G. Sibeck, Upper limits on the contribution of flux transfer events to ionospheric convection, *Geophys. Res. Lett.*, *20*, 2829, 1993.

Newell, P. T., C.-I. Meng, D. G. Sibeck, R. Lepping, Some low-altitude cusp dependencies on the interplanetary magnetic field, *J. Geophys. Res.*, *94*, 8921, 1989.

Newell, P. T., W. J. Wing, C. -I. Meng, E. R. Sanchez, and M. E. Greenspan, Identification of the plasma mantle at low altitude, *J. Geophys. Res.*, *96*, 35, 1991a.

Newell, P. T., W. J. Burke, E. R. Sanchez, C. -I. Meng, M. E. Greenspan, and C. R. Clauer, The low-latitude boundary layer and the boundary plasma sheet at low altitude: Prenoon precipitation regions and convection reversal boundaries, *J. Geophys. Res.*, *96*, 21,013, 1991b.

Nishida, A., T. Mukai, H. Hayakawa, A. Matsuoka, K. Tsuruda, N. Kaya, and H. Fukunishi, Unexpected features of the ion precipitation in the so-called cleft/low-latitude boundary layer region: Association with sunward convection and occurrence on open field lines, *J. Geophys. Res.*, *98*, 11,161, 1993.

Onsager, T. G., C. A. Kletzing, J. B. Austin, and H. MacKiernan, Model of magnetosheath plasma in the magnetosphere: Cusp and mantle particles at low-latitudes, *Geophys. Res. Lett.*, *20*, 479, 1993.

Potemra, T. A., T. Iijima, and N. A. Saflekos, Large-scale characteristics of Birkeland currents, in *Dynamics of the Magnetosphere*, edited by S.-I. Akasofu, p. 165, D. Reidel, Norwell, Mass., 1980.

Primdahl, F., and F. Spangslev, Cusp region and auroral zone field aligned currents, *Ann. Geophys.*, *37*, 529, 1981.

Reiff, P. H., Sunward convection in both polar caps, *J. Geophys. Res.*, *87*, 5976, 1982.

Reiff, P. H., Evidence of magnetic merging from low-altitude spacecraft and ground-based experiments, in *Magnetic Reconnection in Space and Laboratory Plasmas, Geophys. Monogr. Ser.*, vol. 30, edited by E. W. Hones, Jr., p. 104, AGU, Washington, D. C., 1984.

Reiff, P. H., and J. L. Burch, IMF B_y-dependent plasma

flow and Birkeland currents in the dayside magnetosphere, 2, A global model for northward and southward IMF, *J. Geophys. Res.*, *90*, 1595, 1985.

Reiff, P. H., T. W. Hill, and J. L. Burch, Solar wind plasma injection at the dayside magnetospheric cusp, *J. Geophys. Res.*, *82*, 479, 1977.

Rich, F. J., and N. C. Maynard, Consequences of using simple analytical functions for the high-latitude convection electric field, *J. Geophys. Res.*, *94*, 3687, 1989.

Richmond, A. D., Assimilative mapping of ionospheric electrodynamics, *Adv. Space Res.*, *12*, 59, 1992.

Richmond, A. D., and Y. Kamide, Mapping electrodynamic features of the high-latitude ionosphere from localized observations, Technique, *J. Geophys. Res.*, *93*, 5741, 1988.

Rijnbeek, R. P., S. W. H. Cowley, D. J. Southwood, and C. T. Russell, A survey of dayside flux transfer events observed by the ISEE 1 and 2 magnetometers, *J. Geophys. Res.*, *89*, 786, 1984.

Robinson, R. M., R. R. Vondrak, K. Miller, T. Dadds, and D. Hardy, On calculating ionospheric conductances from the flux and energy of precipitating electrons, *J. Geophys. Res.*, *92*, 2565, 1987.

Roeder, J. L., and L. R. Lyons, Energetic and magnetosheath energy particle signatures of the low-latitude boundary layer at low altitude near noon, *J. Geophys. Res.*, *97*, 13,817, 1992.

Russell, C. T., and R. C. Elphic, ISEE observations of flux transfer events at the dayside magnetopause, *Geophys. Res. Lett.*, *6*, 33, 1979.

Saflekos, N. A., J. L. Burch, M. Sugiura, D. A. Gurnett, and J. L. Horwitz, Observations of reconnected flux tubes within the midaltitude cusp, *J. Geophys. Res.*, *95*, 8037, 1990.

Saunders, M. A., The morphology of dayside Birkeland currents, *J. Atmos. Terr. Phys.*, *54*, 457, 1992.

Shelley, E. G., R. D. Sharp, and R. G. Johnson, He^{++} and H^+ flux measurements in the day side cusp: Estimates of convection electric field, *J. Geophys. Res.*, *81*, 2363, 1976.

Siscoe, G. L., and T. S. Huang, Polar cap inflation and deflation, *J. Geophys. Res.*, *90*, 543, 1985.

Siscoe, G. L., W. Lotko, and B. U. O. Sonnerup, A high-altitude, low-latitude boundary layer model of the convection current system, *J. Geophys. Res.*, *96*, 3487, 1991.

Sonnerup, B. U. O., Theory of the low-latitude boundary layer, *J. Geophys. Res.*, *85*, 2017, 1980.

Sonnerup, B. U. O., G. Paschmann, I. Papamastorakis, N. Sckopke, G. Haerendel, S. J. Bame, J. R. Asbridge, J. T. Gosling, and C. T. Russell, Evidence for magnetic field reconnection at the Earth's magnetopause, *J. Geophys. Res.*, *86*, 10,049, 1981.

Taguchi, S., M. Sugiura, J. D. Winningham, and J. A. Slavin, Characterization of the IMF B_y-dependent field-aligned currents in the cleft region based on DE 2 observations, *J. Geophys. Res.*, *98*, 1393, 1993.

Troshichev, O. A., Polar magnetic disturbances and field-aligned currents, *Space Sci. Rev.*, *32*, 275, 1982.

VanZandt, T. E., W. L. Clark, and J. M. Warnock, Magnetic apex coordinates: A magnetic coordinate system for the ionospheric F2 layer, *J. Geophys. Res.*, *77*, 2406, 1972.

Xu, D., M. G. Kivelson, R. J. Walker, P. T. Newell, and C. -I. Meng, Interplanetary magnetic field control of mantle precipitation and associated field-aligned currents, *J. Geophys. Res.*, in press, 1995.

Yamauchi, M., R. Lundin, and J. Woch, The interplanetary magnetic field B_y effects on large-scale field-aligned currents near local noon: Contribution from cusp part and noncusp part, *J. Geophys. Res.*, *98*, 5761, 1993.

Zanetti, L. J., T. A. Potemra, J. P. Doering, J. S. Lee, J. F. Fennel, and R. A. Hoffman, Interplanetary magnetic field control of high-latitude activity on July 29, 1977, *J. Geophys. Res.*, *87*, 5963, 1982.

G. Burns and R. Morris, Australia Antarctic Division, Kingston, Tasmania, Australia.

O. de la Beaujardiére, SRI, Menlo Park, CA 94025.

W. F. Denig and F. J. Rich, Phillips Laboratory, Hanscom Air Force Base, MA 01731.

E. Friis-Christensen, Danish Meteorological Institute, Copenhagen 2791, Denmark.

H. W. Kroehl, National Geophysical Data Center, NOAA, Boulder, CO 80307.

G. Lu, High Altitude Observatory, NCAR, Boulder, CO 80307-3000.

L. R. Lyons, The Aerospace Corporation, Los Angeles, CA 90009.

A. McEwin, Australian Geological Survey Organisation, Canberra 2601, Australia.

P. T. Newell and J. M. Ruohoniemi, Applied Physics Laboratory, Johns Hopkins University, Laurel, MD 20723.

H. Opgenoorth and M. A. L. Persson, Swedish Institute of Space Physics S-75590, Sweden.

P. H. Reiff, Department of Space Physics and Astronomy, Rice University, Houston, TX 77251.

L. Tomlinson, Institute of Geological and Nuclear Sciences, Christchurch, New Zealand.

(Received May 3, 1994; revised August 29, 1994;
accepted October 6, 1994.)